

Excitonic phases in a spatially separated electron-hole ladder model

DinhDuy Vu¹ and Sankar Das Sarma¹

¹*Condensed Matter Theory Center and Joint Quantum Institute,
Department of Physics, University of Maryland, College Park, Maryland 20742, USA*

We obtain the numerical ground state of a one-dimensional ladder model with the upper and lower chains occupied by spatially-separated electrons and holes, respectively. Under charge neutrality, we find that the excitonic bound states are always formed, i.e., no finite regime of decoupled electron and hole plasma exists at zero temperature. The system either behaves like a bosonic liquid or a bosonic crystal depending on the inter-chain attractive and intra-chain repulsive interaction strengths. We also provide the detailed excitonic phase diagrams in the intra- and inter-chain interaction parameters, with and without disorder.

Introduction - Electrons and holes can form bound states through the attractive Coulomb interaction, called excitons. At sufficiently low temperatures, excitons can condense due to their bosonic nature [1–5]. One exciting experimental possibility is the 2D electron-hole bilayer, where the attraction between the electrons in one layer and the holes in the other layer should lead to interlayer coherent excitonic bosonic condensation [6–10]. This effect results in measurable effects, including enhanced exciton mobility, increased radiative decay rate, and photoluminescence noise. Recently, transport evidence has been reported for bilayered exciton condensation in several different layered systems [11–13]. There is also extensive experimental literature on the closely related phenomenon of spontaneous interlayer coherence in bilayer quantum Hall systems with a total filling of unity, where the electron-hole transformation in a filled Landau level produces an effective exciton condensate [14–16]. In spite of very extensive theoretical literature on the subject, the central conceptual issue of the $T = 0$ ground-state quantum phase diagram of the electron-hole bilayers remains problematic since even the basic question of the allowed $T = 0$ quantum phases remain unknown and controversial. Many publications claim uncritically that the $T = 0$ phase contains the unpaired electron-hole liquid as a possible ground state with a (Mott-like) quantum phase transition from the bosonic exciton liquid to the fermionic electron-hole liquid at weak coupling – see the discussion and citations in [17]. We believe this claim to be incorrect, and there is no ground state transition to an electron-hole liquid in bilayer electron-hole systems (or quantum Hall bilayers at a filling factor of unity).

In this work, we theoretically investigate, using exact diagonalization, a two-chain 1D version of 2D bilayers – a ladder model with two oppositely charged spatially-separated 1D chains. Our system is controlled by two parameters, the intra-chain repulsive interaction U_1 and inter-chain attractive interaction U_2 . We are particularly interested in the (U_1, U_2) phase diagram and the important issue of how many phases it can have. To answer this question, we numerically simulate the

ground state using the DMRG method implemented by the ITensor package [18, 19], which is essentially an exact technique for our purpose.

Intuitively, one might hypothesize a plasma phase when the electrons and holes are concentrated densely enough in their respective channels. In the other limit, the electron-hole interaction should prevail, making the elementary excitations primarily excitons. We find that there is no such electron-hole liquid phase, and excitons are always favored in the ground state for any non-zero attractive interaction, with the excitons at low U_2 having a large size and propagating only for a short distance. Additionally, we observe the crystallization of the bosonic liquid for large U_1 , resulting in a phase diagram only having two phases: an excitonic bosonic liquid and a crystal. We also study the robustness of this phase diagram against disorder.

Model Hamiltonian - The ladder model is defined by

$$H_0 = - \sum_i (c_{i+1}^\dagger c_i + \bar{c}_{i+1}^\dagger \bar{c}_i + h.c.) + U_1(n_{i+1}n_i + \bar{n}_{i+1}\bar{n}_i) - U_2(n_i\bar{n}_i). \quad (1)$$

Here, c_i (\bar{c}_i) is the annihilation operator for the electron (hole) at site i of the upper (lower) chain. We fix the intra-chain hopping strength to be unity and $U_2, U_1 > 0$ corresponding to the (electron-hole) attractive and (electron-electron or hole-hole) repulsive interaction within and between chains. Note that we ignore any interchain tunneling, and the Pauli principle is explicitly incorporated in Eq. (1) since we ignore spins as a nonessential complication for the physics of exciton condensation. Throughout this work, we also fix the filling of each chain to be $1/2$ and use the periodic boundary condition. For $U_2 = 0$, each chain has an electron (hole) liquid, which is a Luttinger liquid (but this is not relevant for the physics of our interest where the focus is on the inter-chain bosonic correlations for non-zero U_2).

To characterize the bosonic nature of the system, we compute the following correlation functions

$$C^*(i', i) = \langle c_{i'} \bar{c}_i \bar{c}_i^\dagger c_i^\dagger \rangle, \quad C(i', i) = \langle c_{i'} c_i^\dagger \rangle \quad (2)$$

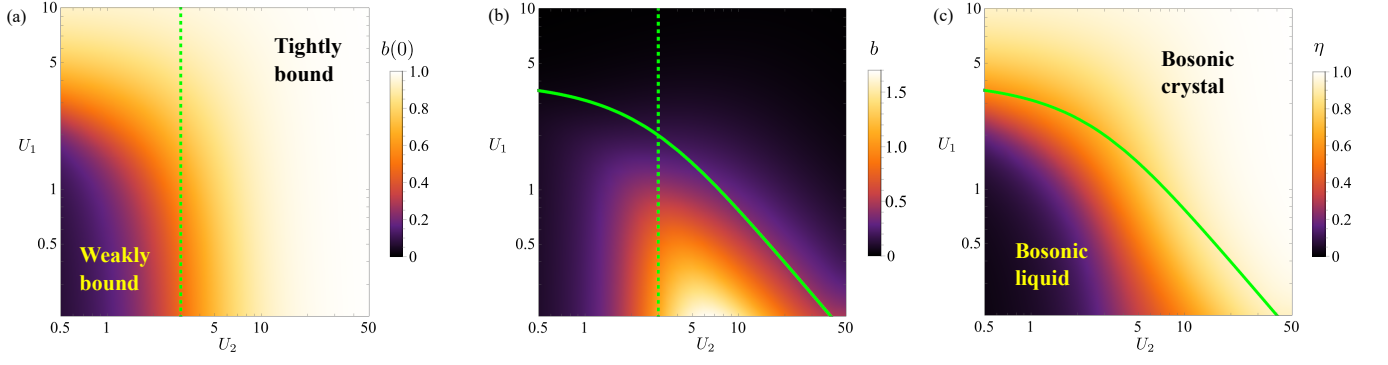


FIG. 1. (U_1, U_2) phase diagram for a 14-rung ladder system. (a) Onsite bosonic correlation $b(0)$. (b) Long-range bosonic correlation $b = \sum_{r=1}^{L/2} b(r)$. (c) Crystalline order parameter from the bosonic density-density correlation. The dashed line given by $U_2 = 3$ separates the weakly bound ($b(0) < 0.5$) and tightly bound ($b(0) > 0.5$) exciton regimes at weak U_1 . The solid green line given by $\sqrt{16 + U_2^2} - U_2 = U_1$ separates the bosonic crystal and bosonic liquid.

where C^* is the double-chain propagation involving moving a hole and an electron simultaneously, while C is the single-chain electron propagation (hole propagation \bar{C} is defined similarly). When the two chains are decoupled, i.e. $U_2 = 0$, $C^*(i', i) = C(i', i)\bar{C}(i', i)$ so the difference

$$b(r) = 4L^{-1} \sum_{i=1}^L |C^*(i+r, i) - C(i+r, i)\bar{C}(i+r, i)| \quad (3)$$

indicates the bosonic correlator for the exciton propagation. The numerical coefficient 4 is chosen so that $b(0) = 1$ in the maximally coupled limit $U_2 \rightarrow \infty$ where every rung is either empty or occupied by one exciton, i.e., no uncoupled electrons or holes. Indeed, in this limit, $C^*(i, i)$, $C(i, i)$, $\bar{C}(i, i)$ that count the onsite occupancy of excitons, electrons, and holes, all read $1/2$ due to the half-filling and charge-neutrality conditions. The quantity $b(0)$ thus indicates how strong the electron-hole bound state or equivalently the bosonic correlation is.

In Fig. 1(a), we show $b(0)$ as a function of interaction strengths U_1 and U_2 in a 14-rung ladder system, i.e. 28 particles, with $b(0) > 0$ for any non-zero U_2 . For small U_1 , the exciton becomes tightly bound for $U_2 \gtrsim 3$, resulting in a vertical crossover. For large U_1 , $b(0)$ saturates trivially because the strong repulsive U_1 induces independent Wigner crystals on the two chains, and any $U_2 > 0$ can lock these crystals with each other. We dubbed the resultant state coherent Wigner crystal (CWC) because of the locking of the two crystals due to non-zero (albeit small) U_2 .

The bosonic correlation also has information about the mobility of the exciton bound state, which is encoded in $b = \sum_{r=1}^{L/2} b(r)$ shown in Fig. 1(b). At small U_1 and U_2 , the onset of long-range bosonic correlation coincides with the formation of bosonic bound states. However, the exciton mobility vanishes at larger U_2 even where $b(0)$ clearly indicates the existence of strongly bound excitons.

This is because excitons in our model are really hardcore bosons, which behave similarly to fermions in one dimension and tend to localize (rather than condense) under a repulsive interaction. This feature is specific to our 1D model and would not apply to 2D bilayers. To estimate the localization crossover in this large U_2 limit, we consider a simplified half-filled 2-rung ladder with $U_1 = 0$. The energy spectrum can be obtained by solving the 4×4 matrix

$$h = \begin{pmatrix} -U_2 & 1 & 1 & 0 \\ 1 & 0 & 0 & 1 \\ 1 & 0 & 0 & 1 \\ 0 & 1 & 1 & -U_2 \end{pmatrix} \quad (4)$$

The ground state and first excited state energies are $E_0 = -(U_2 + \sqrt{16 + U_2^2})/2$ and $E_1 = -U_2$, from which we can estimate the renormalized hopping strength of an exciton as

$$t^* = (E_1 - E_0)/2 = (\sqrt{16 + U_2^2} - U_2)/4. \quad (5)$$

The bosonic liquid crosses over to the solid when $t^* \propto U_1$ (we demonstrate $t^* = U_1/4$ in Fig. 1(b)). For $U_2 \rightarrow 0$, the crossover happens at $U_1 = \mathcal{O}(1)$ while in the limit $U_2 \rightarrow \infty$, $U_1 \propto 1/U_2$. These analytical conditions for the transitions to the solid phase (for $U_1 \gg 1$ and $U_2 \gg 1$) agree with our numerical results, allowing us to draw a putative line between the bosonic liquid and the bosonic solid. We believe this transition to be an effective first-order solid-liquid transition for the exciton system.

To confirm our statement that the bosonic liquid can crystalline under repulsive interaction, we directly compute the crystalline modulation in the inter-chain density-density correlation

$$\eta = \frac{2}{L[L/4]} \sum_{i=1}^L \sum_{j=0}^{L/2} (-1)^j \langle \bar{n}_i n_{i+j} \rangle. \quad (6)$$

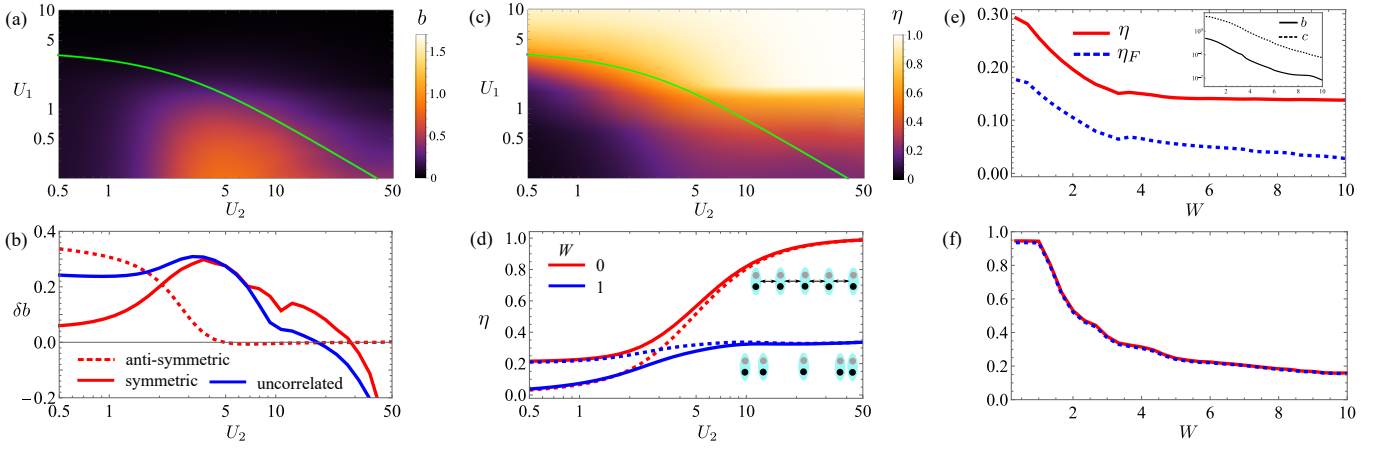


FIG. 2. (a) Bosonic long-range correlation under uncorrelated disorder and fixed $W = 1$, the crossover line is carried over from the pristine system. (b) Relative deviation induced by three disorder models having the same $W = 1$ along the line $U_1 = 0.5$. (c) The crystalline order of the disordered system is similar to (a). (d) Comparison between η (solid) and η_F (dashed), showing the inter-chain synchronization happens at the same U_2 . (e, f) η and η_F for $U_1 = 0.5, U_2 = 2$ (e) and $U_1 = 2, U_2 = 10$ (f). The inset in (e) shows that the bosonic and fermionic correlations decay concomitantly with W .

We note that the alternating sign is compatible with the half-filled crystal, and the normalization guarantees $\eta = 1$ for the maximally crystallized state. Figure 1(c) clearly shows that the vanishing of exciton mobility almost coincides with the formation of bosonic crystals. The very slight mismatch can be explained by Eq. (4). Accordingly, the total energy of two excitons (four fermions) $E_{\text{pair}} = -2U_2 > E_1 + E_0$. This means, even without the long-range U_1 , two excitons have an exchange-like repulsive interaction in the same order as the kinetic energy. Therefore, the strongly-bound bosonic liquid has non-zero crystalline order even though the electrons and holes have no intrinsic repulsive interaction. This explains why the crystalline order emerges earlier than the vanishing of the bosonic liquid phase. The bosonic solid-liquid phase boundary, together with the weakly (small U_2) to strongly (large U_2) bound states, partition the (U_1, U_2) parameter space into four regimes. The bosonic liquid is separated into the weakly and strongly bound BEC – the so-called BCS-BEC crossover. Similarly, the bosonic crystal phase can be subdivided into the CWC and dipolar crystal (DC). CWC and DC are not different phases and differ only quantitatively, depending on whether the state is induced by introducing weak U_2 between the two Wigner crystals or U_1 on the liquid phase of strongly bound excitons.

One remaining question is whether the weakly bound exciton survives or is replaced by electron/hole plasma in the thermodynamic limit. We perform a finite-size scaling analysis (shown in the SM [20]) and observe a convergence with system size, which supports the claim that excitons always form for any attractive interaction $U_2 > 0$, and there is no Mott transition for any finite U_2 .

Disordered phase diagram - We study the robustness of

the phase diagram under random disorder, i.e., $H = H_0 + \sum_i W_i n_i + \bar{W}_i \bar{n}_i$. The disorder value at each site is drawn independently from a uniform distribution $(-W, W)$.

In Fig. 2(a) and (c), we reproduce the phase diagram under uncorrelated noise with amplitude $W = 1$. This noise dampens the long-range bosonic correlation (Fig. 2(a)) and generates a peculiar regime around the crossover line for $U_1 < 2$ where the bosons are nearly immobile ($b \sim 0$) but do not crystallize either ($\eta < 1$). Our current model assumes no correlation between the disorder on the upper and lower chains. We can, however, gain some insight from studying the problem using two complementary limits, i.e., the disorders on the two chains are (i) anti-symmetric ($W_i = -\bar{W}_i$) or (ii) symmetric ($W_i = \bar{W}_i$).

In Fig. 2(b), we show the relative deviation on the long-range bosonic correlation $\delta b = (b_0 - b_W)/b_0$ where b_W is computed at disorder strength W (and fixed $U_1 = 0.5$). Despite having the same disorder amplitude $W = 1$, the three disorder models behave differently. The anti-symmetric disorder is relevant for the weak-coupling U_2 but negated by sufficiently large U_2 . The anti-symmetry of the disorder model tends to localize electrons and holes at different rungs (a local potential minimum in one chain corresponds to a local maximum in the adjacent), directly competing with the effect of the inter-chain attraction that prefers both an electron and a hole on one rung. For stronger U_2 , the elementary particles are point-like composite bosons, and the net potential felt by this object is vanishing, resulting in robustness against disorder.

By contrast, the system is more susceptible to symmetric disorder in the strong-coupling U_2 limit. In this limit, the net potential the boson feels is non-

zero and $\sim W$. At the same time, the effective hopping is suppressed by U_2^{-1} , resulting in the enhanced sensitivity to symmetric disorder for large U_2 . Returning to our original uncorrelated disorder model, it can be decomposed into anti-symmetric and symmetric components. Therefore, for small U_2 , the disorder affects the system by separately localizing electrons and holes (similar to anti-symmetric disorder). For large U_2 , the main effect is the localization of tightly-bound bosons (electrons and holes localized at adjacent sites similar to symmetric disorder). This observation explains the irregular localized regime mentioned in Fig. 2(b). This is the Bose glass regime induced by disorder (for $U_2 > 5$ in Fig. 2b), where bosons are localized but lacking any long-range order.

With the introduction of uncorrelated disorder, the two chains are not equivalent (per each random disorder configuration), so we introduce two additional order parameters, which are the intra-chain version of b and η

$$c = 4L^{-1} \sum_{r=1}^{L/2} \sum_{i=1}^L |C(i+r, i) \bar{C}(i+r, i)| \quad (7)$$

$$\eta_F = \frac{2}{L[L/4]} \sum_{i=1}^L \sum_{j=0}^{L/2} (-1)^j \langle n_i n_{i+j} \rangle.$$

In Fig. 2(d), we compare η and η_F in the pristine and disordered cases at fixed $U_1 = 0.5$. The convergence of these two quantities indicates the synchronization between the two chains, which happens around the same U_2 for both cases. However, in the pristine case, η and η_F are both saturated, but not in the disordered case. The correspondent boson localization landscapes are pictorially shown in Fig. 2(d) with the long-range order present (absent) in the pristine (disordered) system.

The previous results are all given for $W = 1$. We now study whether stronger disorder can destroy inter-chain coherence. In Fig. 2(e), we show the effect of disorder on the bosonic liquid phase ($U_1 = 0.5, U_2 = 2$). It is clear from the inset that b is suppressed exponentially by W , but the intra-chain counterpart c also decays just as fast. This shows that the bosonic correlation is destroyed at the same time as the underlying Fermi surface, and there cannot exist any decoherent Luttinger liquid phase by introducing disorder. Additionally, η and η_F stay distinct for any W , clarifying that the large- W state is two independent Anderson insulators. On the other hand, starting with the bosonic crystal ($U_1 = 2, U_2 = 10$), η and η_F decrease but remain identical, showing a transition from bosonic crystal to bosonic glass. Thus, as W increases, the bosonic liquid becomes decoherent Anderson insulators, while the bosonic crystal loses the long-range order and becomes bosonic glass. In the limit $W \rightarrow \infty$, the entire parametric phase is trivially decoupled electron/hole Anderson insulators.

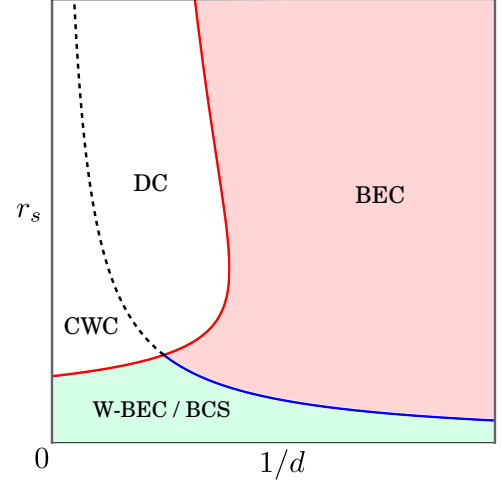


FIG. 3. Schematic phase diagram of indirect excitons in 2D bilayers. The red line given by Eq. (8) separates the crystalline and liquid phases, and the blue line given by $r_s \sim d$ separates the strongly bound exciton BEC phase from the weakly-bound BEC (W-BEC) or the BCS phase. The extension of the blue line into the crystalline phase (dashed lines) indicates the dipolar crystal (DC) and the coherent Wigner crystal (CWC) phases. There is no electron-hole plasma phase at $T = 0$.

Conclusion - We have calculated the quantum phase diagram of indirect excitons formed between two oppositely charged spatially separated 1D wires. This setup lets us directly tune the binding energy and measure various correlation functions. At zero temperature, excitons are always formed, and the entire parameter space is partitioned into the bosonic liquid and bosonic crystal phases. Upon introducing a small disorder, the bosonic characteristic remains unchanged, with the bosonic crystal phases transitioning into a bosonic Anderson insulator. At finite T , there can indeed be an electron-hole liquid phase, particularly for small U_2 where the exciton binding is weak [20].

From our 1D tight-binding 2-channel ladder model, we propose some features of the continuum excitons, potentially realized in 2D bilayer systems. The kinetic and intra-layer repulsive interaction is governed by the electron/hole density so that $t \sim 1/r_s^2$ and $U_1 \sim 1/r_s$. Here we use the convention $r_s = a$ with a being the average inter-particle spacing within one layer normalized by the Bohr radius. U_2 in our model becomes $1/d$ with dimensionless d the inter-layer separation also scaled by the Bohr radius. There are two differences with our tight-binding model. First, the exciton kinetic energy (or that of the electron-hole pair center of mass) remains finite for strong U_2 and only depends on r_s . Additionally, the interaction in the strong- U_2 limit becomes a dipolar $1/r^3$ interaction. Note that the strong U_2 limit is different in 2D bilayers compared with 1D since hard-core bosons

are no longer equivalent to fermions. We estimate a phase diagram as shown in Fig. 3 where the qualitative phase boundary is mostly likely crossover in 1D and true phase transition in 2D. The solid-liquid phase boundary is sketched as follows

$$\frac{1}{r_s} - \frac{1}{\sqrt{r_s^2 + d^2}} = \frac{C}{r_s^2} \quad (8)$$

with the LHS being the repulsive interaction energy, RHS the kinetic energy (electrons/holes and excitons), and C a constant. On the other hand, the exciton description apparently prevails when $d \ll a$ or $r_s \gg d$. We note that the asymptotic Eq. (8) yield $r_s \sim d^2 \gg d$ in the large- d limit, so similar to the tight-binding model, the solid phase may qualitatively be divided into the coherent Wigner crystal and dipolar crystal phases depending on the value of r_s/d . In the SM, we perform a numerical simulation with attractive long-range interaction to capture the dipole physics [20]. Remarkably, a part of this proposed phase diagram is realized in our dipolar 1D tight-binding model, with the main difference being the large U_2 regime.

Acknowledgments - The authors are grateful for helpful discussions and communications with Professors Jay Deep Sau, Bert Halperin, Peter Littlewood, Kin Fai Mak, Fengcheng Wu, and Jim Eisenstein. This work is supported by Laboratory for Physical Sciences. The authors acknowledge the University of Maryland supercomputing resources (<https://hpcc.umd.edu>) made available for conducting the research reported in this paper.

[1] L. V. Keldysh and Y. V. Kopaev, Fiz. Tverd. Tela **6**, 2791 (1964), [Sov. Phys. Solid State 6,2219 (1965)].

[2] A. N. Kozlov and L. A. Maksimov, Zh. Eksp. Teor. Fiz. **48**, 1184 (1965), [Sov. Phys. JETP 21,790 (1965)].

[3] L. V. Keldysh and A. N. Kozlov, Eksp. Teor. Fiz. **54**, 978 (1968), [Sov. Phys. JETP 27, 521 (1968)].

[4] C. Comte and P. Nozieres, J. Phys. France **43**, 1069 (1982).

[5] P. Nozieres and C. Comte, J. Phys. France **43**, 1083 (1982).

[6] Y. E. Lozovik and V. I. Yudson, Pisma v Zh. Eksp. Teor. Fiz. **22**, 556 (1975), jETP Lett. 22,274 (1975).

[7] S. I. Shevchenko, Fiz. Nizk. Temp. **2**, 505 (1976), [Sov. J. Low Temp. Phys. 2, 251 (1976)].

[8] X. Zhu, P. B. Littlewood, M. S. Hybertsen, and T. M. Rice, Phys. Rev. Lett. **74**, 1633 (1995).

[9] P. B. Littlewood and X. Zhu, Phys. Scr. **1996**, 56 (1996).

[10] X. Zhu, M. S. Hybertsen, and P. B. Littlewood, Phys. Rev. B **54**, 13575 (1996).

[11] M. L. Davis, S. Parolo, C. Reichl, W. Dietsche, and W. Wegscheider, Josephson-like tunnel resonance and large coulomb drag in gaas-based electron-hole bilayers (2023), arXiv:2304.06691 [cond-mat.mes-hall].

[12] Z. Wang, D. A. Rhodes, K. Watanabe, T. Taniguchi, J. C. Hone, J. Shan, and K. F. Mak, Nature **574**, 76 (2019).

[13] L. Ma, P. X. Nguyen, Z. Wang, Y. Zeng, K. Watanabe, T. Taniguchi, A. H. MacDonald, K. F. Mak, and J. Shan, Nature **598**, 585 (2021).

[14] J. P. Eisenstein, Annu. Rev. Condens. Matter Phys. **5**, 159 (2014).

[15] J. P. Eisenstein, L. N. Pfeiffer, and K. W. West, Phys. Rev. Lett. **123**, 066802 (2019).

[16] X. Liu, J. I. A. Li, K. Watanabe, T. Taniguchi, J. Hone, B. I. Halperin, P. Kim, and C. R. Dean, Science **375**, 205 (2022).

[17] F.-C. Wu, F. Xue, and A. H. MacDonald, Phys. Rev. B **92**, 165121 (2015).

[18] M. Fishman, S. R. White, and E. M. Stoudenmire, SciPost Phys. Codebases , 4 (2022).

[19] M. Fishman, S. R. White, and E. M. Stoudenmire, SciPost Phys. Codebases , 4 (2022).

[20] See Supplemental Material for Finite-size scaling, Effect of finite temperature, and Long-range attractive potential.

Supplemental Material for “Excitonic phases in a spatially separated electron-hole ladder model”

I. Finite-size scaling

In this section, we perform the finite-size scaling analysis with respect to Fig. 1 of the main text in Fig. 1. The results converge with system sizes, consistent with the fact that there is no actual phase transition in 1D, and all transitions are essentially crossover. Nevertheless, it is also true that a fermionic plasma phase does not exist for any non-zero U_2 , reinforcing the central claim of our work.

II. Effect of finite temperature

This section studies the thermal melting and crossover to classical phases at low ($T \ll 1$) and high ($T \sim U_1, U_2$) temperatures. For low temperatures, we compute the first 29 excited states and take the thermal average of observables

$$\langle O \rangle_\beta = \frac{\text{Tr}(e^{-\beta H} O)}{\text{Tr}(e^{-\beta H})} \approx \frac{\sum_{i=0}^{29} e^{-\beta E_i} \langle \psi_i | O | \psi_i \rangle}{\sum_{i=0}^{29} e^{-\beta E_i}}, \quad (1)$$

which enter the correlation functions in the main text. We note that the chemical potential does not appear because we explicitly impose particle number conservation on each chain.

For high temperatures $\beta \approx 0$, we use the stochastic sampling method combined with imaginary time evolution. We first set the initial state by assigning the particles (fixed particle numbers on each chain) to a set of randomly chosen single-particle levels ($U_1 = U_2 = 0$) so that the initial state ensemble consists of orthonormal Slater states. We then evolve the state using the TDVP method and compute the observable expectation value at imaginary time $\tau = \beta/2$. The thermal expectation value is obtained by averaging over the ensemble of initial states as

$$\langle O \rangle_\beta = \frac{\text{Tr}(e^{-\beta H} O)}{\text{Tr}(e^{-\beta H})} \approx \frac{\sum_{i=1}^N \langle \psi_i | e^{-\beta H/2} O e^{-\beta H/2} | \psi_i \rangle}{\sum_{i=1}^N \langle \psi_i | e^{-\beta H} | \psi_i \rangle} \quad (2)$$

which we choose $N = 200$ and has numerically justified the convergence.

For temperatures lower than exciton binding energy (blue and light blue lines), the onsite correlation $b(0)$ is unaffected (Fig. 2(a)), but the long-range bosonic correlation decreases (increases) compared to the zero-temperature bosonic liquid (crystal) phase (Fig. 2(b)). This is consistent with the thermal melting of the bosonic crystal into a bosonic liquid phase, which is further supported by Fig. 2(c) with η approaching η_F but not saturating as U_2 increases. On the other hand, nearest-neighbor U_1 (as compared to the onsite U_2) can recover the crystalline order and increase the melting temperature, as can be seen in Fig. 2(d). Bosonic phases are only destroyed when the temperature exceeds the exciton binding energy, replaced by classical electron and hole plasma. Thus, at finite T , there can indeed be an electron-hole liquid phase, particularly for small U_2 where the exciton binding is weak.

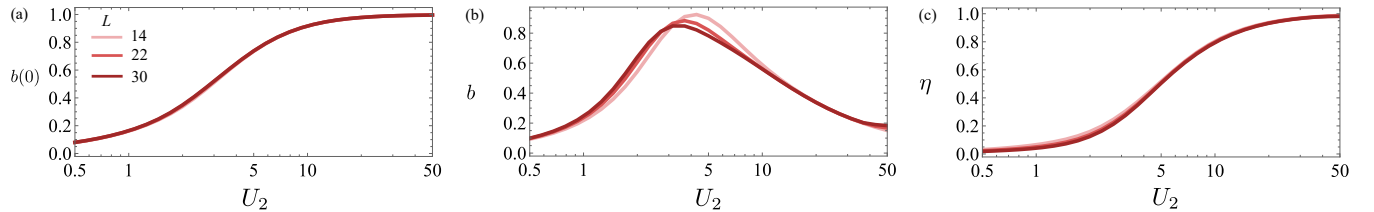


FIG. 1. Finite-size scaling analysis of (a) $b(0)$, (b) b , and (c) η at $U_1 = 0.5$. L is the number of rungs in the ladder model.

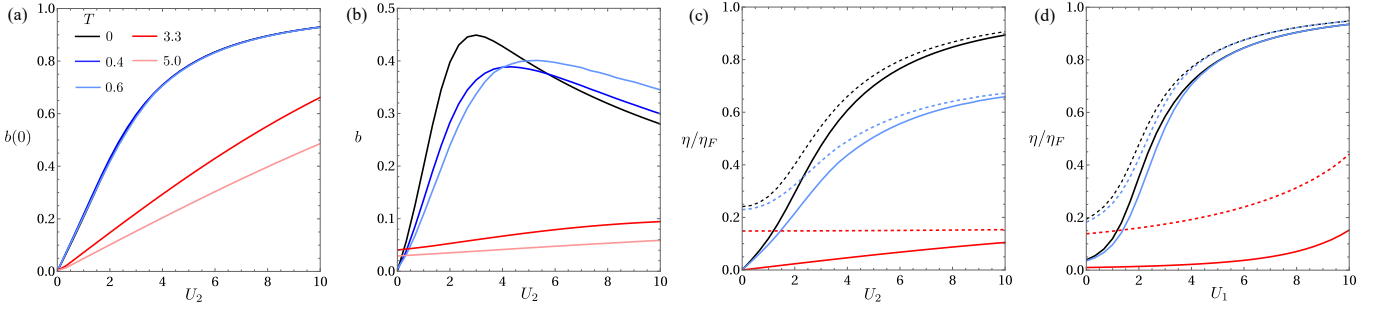


FIG. 2. (a) Onsite bosonic correlation, (b) long-range bosonic correlation. (c-d) Excitonic (solid lines) and fermionic (dashed lines) crystalline order with respect to U_2 and U_1 . Blue and light blue colors denote low temperatures (less than exciton binding energy), while red and light red denote high temperatures (more than exciton energy).

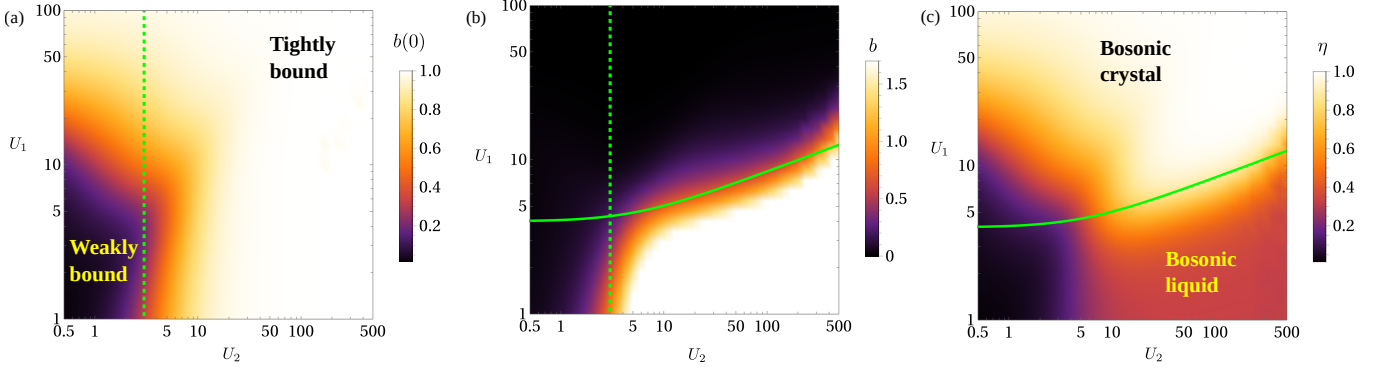


FIG. 3. (U_1, U_2) phase diagram for a 14-rung ladder system with long-range inter-chain attractive and intra-chain repulsive interactions. (a) Onsite bosonic correlation $b(0)$. (b) Long-range bosonic correlation. (c) Crystalline order parameter from the bosonic density-density correlation. The dashed line given by $U_2 = 3$ separates the weakly bound ($b(0) < 0.5$) and tightly bound ($b(0) > 0.5$) exciton regimes at weak U_1 . The solid green line given by Eq. (4) with $C = 1$ separates the bosonic crystal and bosonic liquid. Note that the large U_2 (and small U_1) regime for the dipolar model here is qualitatively different from that in the adjacent attractive interaction model of Fig. 1 in the main text.

III. Long-range attractive potential

We modify the interaction potential into

$$H_I = \sum_i U_1 n_i n_{i+1} + \frac{U_1}{2\gamma} n_i n_{i+2} - \frac{U_2}{2} n_i \bar{n}_i - \frac{U_1 U_2}{(U_1^{2/\gamma} + U_2^{2/\gamma})^{\gamma/2}} n_i \bar{n}_{i+1} - \frac{U_1 U_2}{(U_1^{2/\gamma} + 4U_2^{2/\gamma})^{\gamma/2}} n_i \bar{n}_{i+2} \quad (3)$$

We limit the interaction range to next-nearest sites and choose $\gamma = 1.2$ to avoid unintended frustration. We assume the elementary interaction scales as $1/r^\gamma$ so that $U_1 = a^{-\gamma}$ and $U_2 = d^{-\gamma}$. The other interaction terms are computed from the respective geometrical distances. In Fig. 3, we show an equivalence of Fig. 1 in the main text. The main difference with the system in the main text is that the long-range interaction modifies the solid-liquid phase boundary into

$$\sqrt{16 + U_2^2} - U_2 = C U_1 \left(1 - \frac{U_2}{(U_1^{2/\gamma} + U_2^{2/\gamma})^{\gamma/2}} \right), \quad (4)$$

where the RHS is the nearest-neighbor dipole interaction. We can see that in the limit $U_2 \rightarrow \infty$, the hopping is renormalized to $t^* \sim 1/U_2$, while interaction now becomes dipole-dipole interaction and reads $U_1^3/U_2^2 \ll t^*$. As a result, the large- U_2 regime is dominated by the BEC phase, unlike the crystal phase in Fig. 1 where large U_2 converts the effectively hard core bosonic system to a crystalline fermionic system for $U_2 \gg 1$.